

Article

How to Obtain Maximum Environmental Applicability from Natural Silicates

Daliborka Popadić¹, Nemanja Gavrilov², Ljubiša Ignjatović², Danina Krajišnik³, Slavko Mentus², Maja Milojević-Rakić^{2,*}  and Danica Bajuk-Bogdanović² 

¹ National Laboratory Sector, Department of Organic Residual Analysis, Serbian Environmental Protection Agency, Žabljačka 10A, 11160 Belgrade, Serbia; daliborka.bankovic@sepa.gov.rs

² University of Belgrade-Faculty of Physical Chemistry, Studentski Trg 12-16, 11158 Belgrade, Serbia; gavrilov@ffh.bg.ac.rs (N.G.); ljignjatovic@ffh.bg.ac.rs (L.I.); slavko@ffh.bg.ac.rs (S.M.); danabb@ffh.bg.ac.rs (D.B.-B.)

³ Department of Pharmaceutical Technology and Cosmetology, University of Belgrade-Faculty of Pharmacy, Vojvode Stepe 450, 11221 Belgrade, Serbia; danina.krajsnik@pharmacy.bg.ac.rs

* Correspondence: maja@ffh.bg.ac.rs; Tel.: +381-1121-87133

Abstract: Unmodified natural silicates (bentonite, kaolin, clinoptilolite and diatomites) were tested as adsorbents for the organic pollutants in water tables using Methylene Blue (MB) as the model adsorbate. Among the selected materials, bentonite adsorbed as much as 237 mg/g, confirming its excellent suitability for pollutant removal. Spectral evidence confirmed successful MB immobilization at the bentonite surface. Furthermore, the thermal treatment of MB-saturated adsorbent in an inert atmosphere at 700 °C produced a carbon/silicate composite. EDX confirmed the formation of the nitrogen-doped carbon overlay on the silica scaffold and the obtained composite material was probed as an electrode material for oxygen reduction in an alkaline solution. Reduction proceeded via a two-electron mechanism with the main product being HO₂[−], a known nucleophile, which was subsequently used to degrade/demethylate MB. The composite showed a considerable 70% MB removal rate after an hour of electrochemical treatment. The synergy between the processes of adsorption of MB and the surface-generated HO₂[−] dictates the efficiency of the method and points to a possible route for spent adsorbent reuse in the form of a durable product for environmental protection.

Keywords: bentonite; methylene blue; oxygen reduction reaction; spent adsorbent



Citation: Popadić, D.; Gavrilov, N.; Ignjatović, L.; Krajišnik, D.; Mentus, S.; Milojević-Rakić, M.; Bajuk-Bogdanović, D. How to Obtain Maximum Environmental Applicability from Natural Silicates. *Catalysts* **2022**, *12*, 519. <https://doi.org/10.3390/catal12050519>

Academic Editor: Roman Bulánek

Received: 12 April 2022

Accepted: 4 May 2022

Published: 5 May 2022

Publisher's Note: MDPI stays neutral with regard to jurisdictional claims in published maps and institutional affiliations.



Copyright: © 2022 by the authors. Licensee MDPI, Basel, Switzerland. This article is an open access article distributed under the terms and conditions of the Creative Commons Attribution (CC BY) license (<https://creativecommons.org/licenses/by/4.0/>).

1. Introduction

The search for advanced materials that have favorable properties for the adsorption/degradation of various pollutants from water is still ongoing. Costly, complicated and time-consuming synthesis procedures may not always produce materials with high adsorption capacity/degradation efficiency and therefore the researcher's attention is drawn to the use/modification of abundant and low-cost natural materials [1,2]. In the environmental application field, aluminosilicates represent the most important class of minerals and Earth's crust constituents. Clinoptilolite, hydrated alkali aluminosilicate, is one of the most abundant minerals and is readily available and implemented as incipients/carriers [3–6]. Other crust ingredients are clay minerals with several candidates for targeted applications in adsorption studies. Bentonite is a highly applicable clay [7] mainly composed of montmorillonite, a clay mineral from the smectite group [8]. The characteristics of bentonite depend on the amount of smectite and exchangeable cations in the interlayer space. Due to their structural characteristics of 2:1 tetrahedral SiO₂/octahedral Al₂O₃ layers with substantial voids, bentonites are perceived as good adsorbents. One of the main characteristics of these materials is the swelling ability and high cation exchange capacity. Kaolin's (white clay) main component is kaolinite, a clay mineral of a 1:1 kaolinite group, with tightly distributed tetrahedral and octahedral layers. Diatomites are sedimentary rock silicates that mainly

consist of opal and cristobalite. These materials are light, finely porous rocks consisting mainly of small opal skeletons (or parts thereof) of diatomaceous algae with interesting physico-chemical and biomedical applications [9,10].

Natural material does not necessarily imply efficiency in pollutant removal. Among the affordable and readily available minerals, it is necessary to examine the influence of their different structures, morphologies and composition on adsorption properties, and environmental applicability in general [11,12].

Various dyes were investigated as model pollutants, such as methylene blue (MB), a cationic thiazine dye, which finds its way into essentially different fields—from pharmacology to the dye/textile industry. This multifunctionality arises from versatile functional groups present in its structure. The fact that it can mimic nitrogen/sulfur-containing pollutants in the environment makes MB an excellent candidate for probe testing for resolving environmental threats.

Not only is it important to find an efficient material [13–15] but the question is also what to do with the saturated adsorbent after the adsorption. Materials after adsorption can be further exploited for the preparation of nanoparticles, but this often requires the addition of metal precursors [16]. An attractive approach was proposed by Tian et al. for hydrothermal treatment of dye-saturated palygorskite/Ag nanoparticles. Obtained carbon composites efficiently adsorbed different dyes and pharmaceuticals [17]. Another proposal for spent MB dye biosorbents is their transformation to biochar, which could be subsequently used for additional dye adsorption [18]. MB dye can be used for the functionalization of cellulose gum sorbent to suit the removal of anionic dye [19]. If the intention is shifted toward applications different from reiterating adsorption cycles after burn-off, incorporation of metal ions is necessary, either as a precursor or as a pollutant adsorbate. For instance, a fuel cell setup may benefit from bio sorbent previously used for platinum adsorption [20]. For metal-free electroactive material production, MB is also a good candidate, as graphene dye functionalization leads to highly active and stable electrode material for charge storage application [21].

Here, we propose natural aluminosilicates selection (bentonite, kaolin, clinoptilolite and diatomites) for the adsorption application of MB as a model pollutant in water tables. MB dye removal was studied in detail in the literature employing natural silicates in raw and modified forms [22–28]. Considering that natural samples have different compositions depending on their origin, we examined different samples to find the optimal adsorbent of the highest capacity that can be further processed. Thus, the universal application of the preferred spent adsorbent may be proposed. After carbonization, the selected MB-saturated silicate sample will be used for the electrocatalytic application. Electrochemical dye degradation on various electrode materials is addressed in the literature as an efficient method [29–31]. To establish a comprehensive environmental approach, this novel electrode material will be employed for the degradation of MB in an electrolytic cell by electrogenerated hydroperoxyl radical to extend the lifecycle of such spent adsorbents.

2. Results and Discussion

2.1. Thermal, Spectral and Structural Properties of Investigated Minerals

Thermal profiles of the investigated silicates are given in Figure 1a. Diatomite samples DK and DP are stable with small differences after a physically adsorbed water loss. Kaoline undergoes a phase transformation to metakaolin at around 500 °C [32], while the BE profile consists of two segments, characteristic of smectite mineral. The first step of mass loss up to 200 °C is related to physisorbed water removal, which is followed by dehydration of Ca²⁺ coordinated water and thermal removal of structural OH groups up to over 600 °C [33]. Clinoptilolite displays a continuous mass decrease up to 700 °C in accordance with previous studies [34].

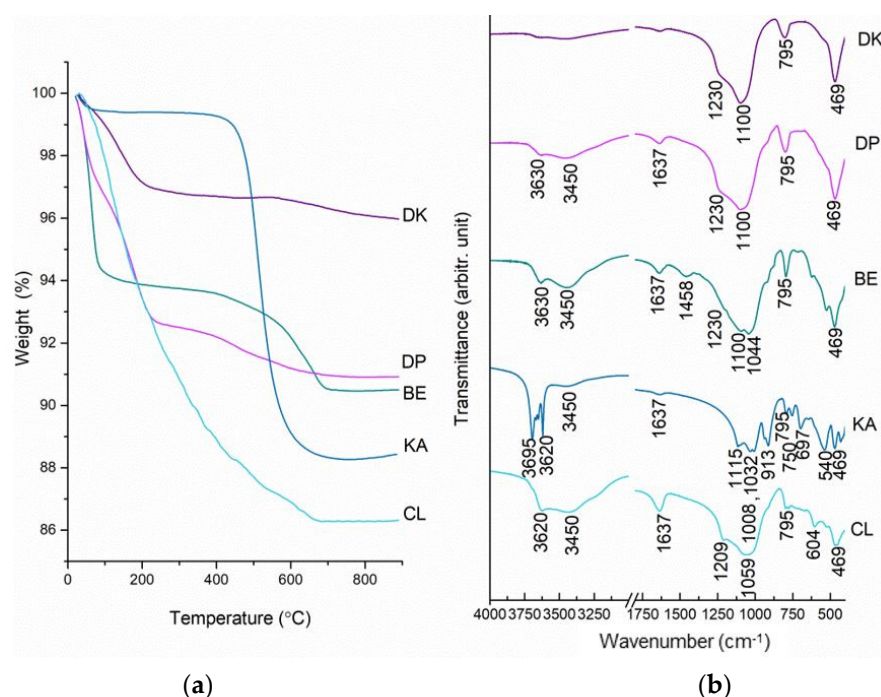


Figure 1. TG profiles (a) and FTIR spectra (b) of natural silicates—clinoptilolite (CL), Peru diatomite (DP), Kolubara diatomite (DK), kaolin (KA) and bentonite (BE).

Spectral profiles of the tested silicates were analyzed and the FTIR spectra are presented in Figure 1b.

In line with the TG results, the diatomite samples DK and DP express the least resolved band at 3450 cm^{-1} and 1637 cm^{-1} attributed to O–H stretching and H–O–H deformation vibration. These bands are evident in the BE and CL samples, accompanied by a sharp band at about 3630 and 3620 cm^{-1} , respectively (stretching of the structural hydroxyl groups). The most complex spectral features in this region are associated with KA, with four resolved bands of the structural OH groups (3695 , 3670 , 3650 and 3620 cm^{-1}) [35], characteristic of the kaolinite mineral, indicating its significant structural ordering.

In addition to the absorption bands of structural OH, Si–O groups play an important role in the differentiation of silicate minerals [36].

The FTIR spectra of the diatomaceous earth samples, DK and DP, give a very strong absorption band at 1100 cm^{-1} with a shoulder at 1230 cm^{-1} attributed to the Si–O–Si stretching vibration. The absorption band at 795 cm^{-1} evolves from the corresponding inter tetrahedral Si–O–Si bending. The absorption peak at around 469 cm^{-1} corresponded to the Si–O–Si bending vibration [37]. The bentonite spectrum reveals strong bands attributed to Si–O elongation in the $1100\text{--}1000\text{ cm}^{-1}$ region, characteristic of the layered montmorillonite structure. The bands corresponding to the Al–Al–OH bending vibrations are observed at 915 cm^{-1} , Al–O–Si at 525 cm^{-1} and Si–O–Si bending vibrations at 469 cm^{-1} . The band at 620 cm^{-1} is assigned to coupled Al–O and Si–O out-of-plane vibrations [38]. The band at 1458 cm^{-1} is assigned to the asymmetric stretching vibration of the present carbonate impurity [39] and other, less pronounced bands in the spectrum originate from clay components. Figure S1 gives a bentonite diffractogram to resolve phase content. Reflections at 6.7° , 19.9° and 35.0° 2θ correspond to the montmorillonite (JCPDS 29-1498), while other reflections correspond to low amounts of feldspar in the form of the albite (JCPDS 09-0466) and quartz phase (JCPDS 46-1045) [40].

The $1120\text{--}1000\text{ cm}^{-1}$ region resolves several strong absorption bands related to Si–O stretching vibrations in the kaolin sample. Two strong bands at 1032 cm^{-1} and 1008 cm^{-1} belong to the antisymmetric in-plane Si–O–Si stretching. The symmetric Si–O stretching band is located at 1115 cm^{-1} while Al₂OH bending modes are positioned at 935 and 913 cm^{-1} ascribed to inner surface/OH groups. Two low-intensity bands at the 750 and

697 cm^{-1} are associated with perpendicular Si–O modes and possibly surface hydroxyls. The Si–O–Al and Si–O–Si bending are located at 540 and 470 cm^{-1} , in that order [41].

In the clinoptilolite spectrum, an intense 1059 cm^{-1} band is ascribed to the asymmetric stretching vibration modes of internal T–O bonds in TO_4 tetrahedra (T = Si and Al). The 795 cm^{-1} and 469 cm^{-1} bands are attributed to the stretching vibration modes of O–T–O groups and the bending vibration modes of T–O bonds, respectively [42].

2.2. Methylene Blue Adsorption-Quantitative, Spectral and Elemental Analysis

The UV–Vis spectrum of MB shows two characteristic absorption bands at 662 and 607 nm with their intensities dependent on the monomer–dimer structure and the dimer development [43]. Low MB concentration up to 70 ppm gives dominantly monomers/dimers, while higher concentrations allow aggregation/stacking, thus changing the spectral profile. As the tested concentration range is rather wide, differences in the intensity ratio of the monomer/dimer band are evident in Figure S2a. Thus, for accurate quantification of MB, the calibration curves are based on the integral band surface instead of the absorbance value.

For MB tested concentrations below 100 ppm, clinoptilolite (CL), diatomite (DP) and bentonite (BE) samples completely and instantly adsorb MB while Kolubara diatomite (DK) and kaolin (KA) enter saturation and therefore, were excluded from further testing. Kaolin's non-expanding structure is fixed without interlayer space, which is the reason for its low adsorption capacity. The CL is getting to its saturation level at 100 ppm while the BE and DP samples retain excellent adsorption performance, (Figure 2a). Furthermore, DP lowered the adsorbed quantity of MB to 54 mg/g, while bentonite demonstrated the best adsorption capacity for the starting MB concentration of 200 ppm. To test the extent of available adsorption sites on bentonite, this sample was further investigated in suspensions with 300, 400 and 500 ppm MB solutions. Complete MB removal was witnessed up to 500 ppm, where 236.6 mg of MB was adsorbed per gram of bentonite adsorbent, approximately 95% of the starting MB quantity. The excellent adsorption performance of bentonite is attributed to its interlayered structure, which is susceptible to expansion and swelling in an aqueous environment, thus forcing the layers apart. To conclude, a mineral from the expanding smectite group is a highly superior adsorbent compared to other tested silicate materials. A cationic dye such as MB readily interacts with clay minerals by cation exchange of extra-framework cations in an aluminosilicate structure [44].

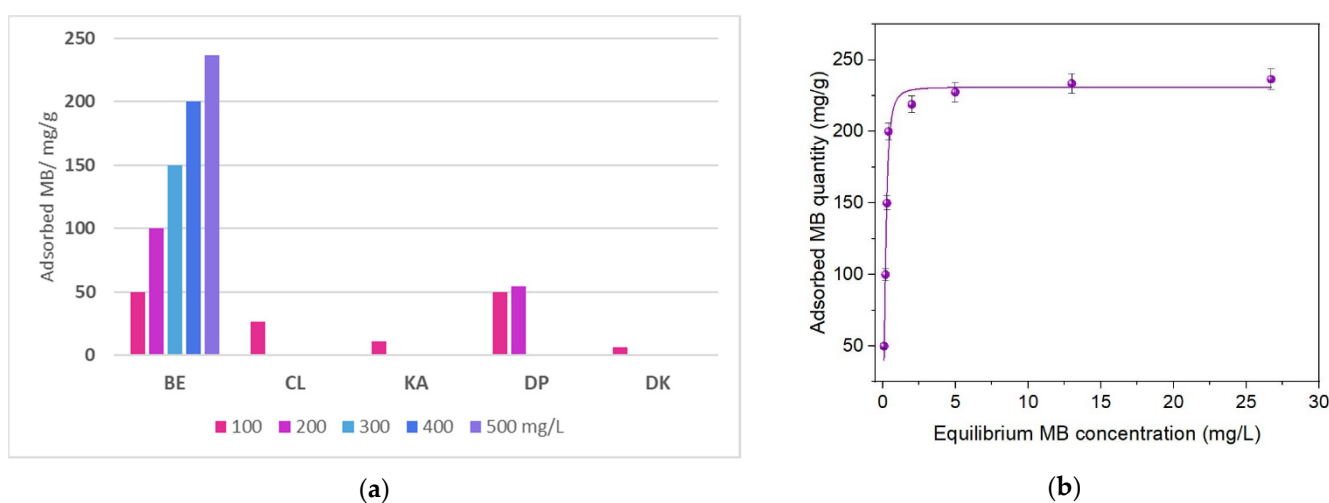


Figure 2. Retained quantities of MB on investigated minerals, recorded for different initial MB concentrations (a); Langmuir–Freundlich adsorption isotherm for MB adsorption on bentonite sample (b).

Adsorption isotherm testing (Figure 2b) for several additional starting MB concentrations revealed the Langmuir–Freundlich isotherm model [45] is better suited for the

description of the adsorption process (correlation coefficient 0.98) in comparison to the less realistic Langmuir equation [45] Yang (correlation coefficient 0.91). This finding is in accordance with presumed nearly equivalent adsorption centers and the excellent adsorption behavior of the bentonite sample.

The MB post-adsorption spectral investigation (Figure 3) reveals no change in the structure of the tested silicates upon adsorption. The most intense pristine MB bands are located at 1592 and 1386 cm^{-1} . These bands can be observed in the BE spectra at 1604 and 1398 cm^{-1} after MB adsorption. The transition of band positions to higher wavenumbers is a result of band shortening due to MB immobilization on the BE surface.

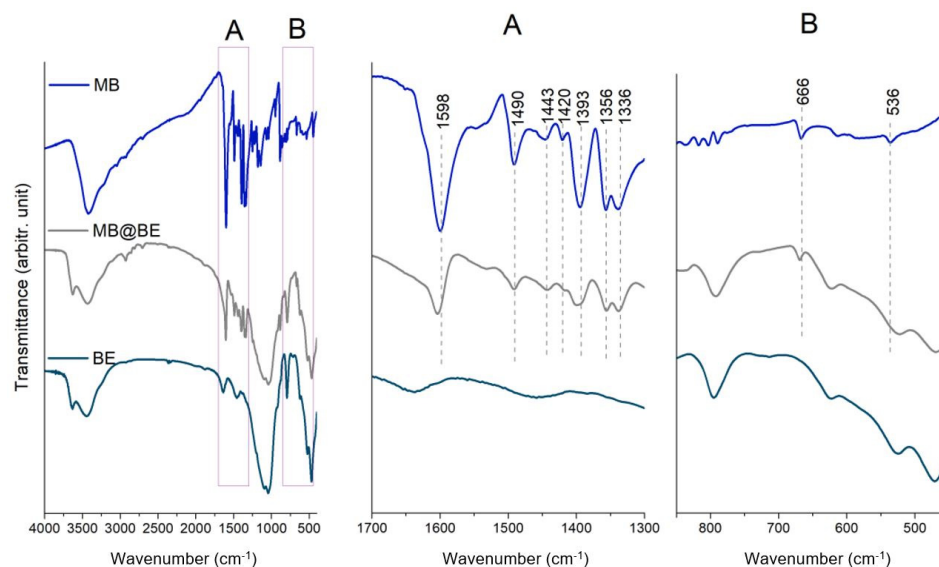


Figure 3. FTIR spectra of MB and BE adsorbent before and after MB adsorption (MB@BE).

As the bentonite sample proved to be the utmost MB adsorbent, carbonization of the saturated adsorbent was the next step in this investigation. In such a way, carbonaceous material comprising heteroatoms was obtained. Raman microanalysis confirmed that the amorphous carbon phase is obtained by thermal treatment of the MB-saturated bentonite sample. The characteristic G (stretching modes, 1585 cm^{-1}) and D (breathing modes, 1373 cm^{-1}) bands are clear indications of MB carbonization with an evident structural disorder [46]. The FTIR spectra give additional information on the preservation of aluminosilicate structure, as witnessed in Figure S3.

To confirm its elemental composition, EDX measurements were performed on the carbonized sample, and the atomic % of dominant elements (>1%) is summarized in Figure 4. The absence of carbon and nitrogen in pristine bentonite is evidenced, while after carbonization, a high portion of the surface is made up of carbon (34 at.%) and nitrogen (7 at.%) atoms. Additionally, the ratio between carbon and nitrogen atoms matches that within the MB molecule. The N-doped carbon phase is evenly present at the aluminosilicate surface in the amount of 25 wt. % carbon and 6 wt. % N, corresponding well to the already-measured highly adsorbed MB quantity.

The favorable elemental composition supports subsequent electroactive testing of this novel material derived from the saturated adsorbent.

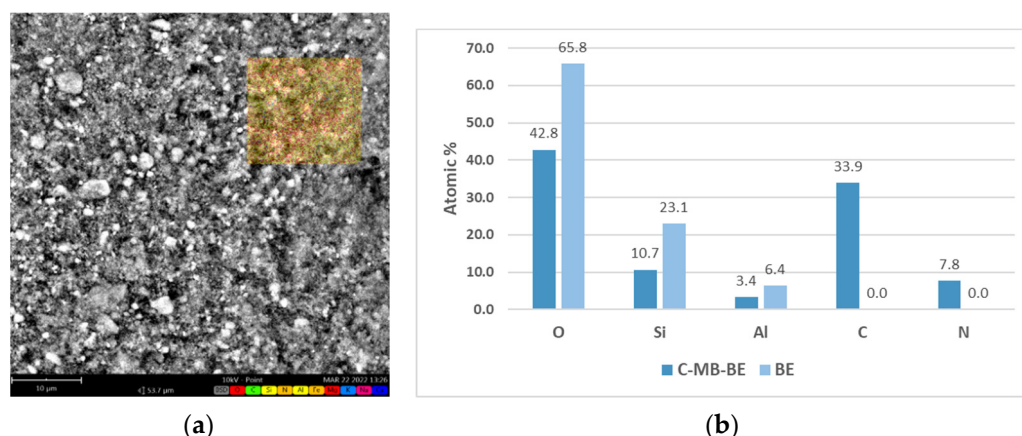


Figure 4. EDX map (a) and elemental composition change for carbonized MB-saturated bentonite (C-MB@BE) in comparison to pristine bentonite (BE) sample (b).

2.3. Electro-Applicability of Spent Adsorbent

After carbonization of the MB dye, adsorbed on bentonite, the silicate scaffold was covered with layers of nitrogen-doped carbon, as seen by Raman, FTIR and EDX. Doped carbons are well known for their activity towards ORR in alkaline solution, albeit somewhat lower than those for transition metals and their oxides [47]. Spent biochar adsorbents of heavy metals can also be transferred to electrocatalysts for ORR [48]. Figure 5 contains the CVs for carbonized saturated adsorbent displaying clear dependence of the measured current on the rate of rotation, indicating that the process of oxygen reduction is diffusion-controlled at more negative potential. Koutecký–Levich (K–L) analysis was conducted to assess the number of exchanged electrons per oxygen molecule and to distinguish between the $2e^-$ – $4e^-$ ORR mechanisms [47,49].

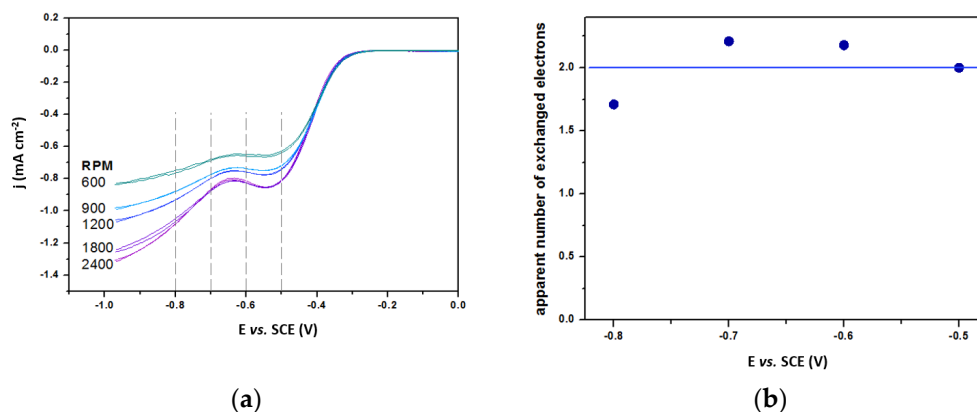


Figure 5. Background-corrected CVs for ORR in 0.1 M KOH at different rotation rates (a); dependence of the apparent number of exchanged electrons on the given potential, according to K–L analysis (b).

Calculated values for the apparent number of exchanged electrons show that $2e^-$ are being consumed in the potential region of interest and that, at a moderately negative potential, HO_2^- is formed according to reaction $\text{O}_2(\text{g}) + \text{H}_2\text{O}(\text{aq}) + 2e^- \leftrightarrow \text{HO}_2^-(\text{aq}) + \text{OH}^-(\text{aq})$.

Katafias et al. [50] investigated chemical MB degradation in base and base/peroxide systems and reported that HO_2^- nucleophile in alkaline solutions may be an efficient phenothiazine derivative degradation agent. This prompted us to check whether electro-generated HO_2^- in the adlayer near or at the electrode surface could be used to reduce MB or degrade it. MB can be involved in a fast, reversible, $2e^-$ redox process where MB transforms to a reduced, colorless leuco-MB form [51] or can be demethylated via nucleophile attack [50,52]. Electron transfer enables versatile applications of MB, which can be followed and analyzed by electrochemical methods [53,54].

After preparation of the initial solution of MB standard in KOH, the potential of the electrode was fixed at an HO_2^- generating potential for three consecutive runs with aliquots taken for spectrophotometric measurements. The UV range monitoring was required to differentiate whether the process is only decolorization (due to colorless leuco-MB evolution) [55] or whether we achieved actual MB degradation and if the formed associated colored degradation products [50,52] decreased. Therefore, withdrawn volumes were used to measure the decrease in absorbance characteristics for both MB species, as presented in Figure 6. The decrease in the spectral response of quiescent KOH/MB (without the electrode present) amounted to 14% after 1 h and served as a baseline/guideline for degradation studies, Figure 6a. Interestingly, there is no rise in the UV absorption band due to MB reduction to leuco-MB. Although not resolved due to the stronger MB signal overlap, this characteristic band at 255 nm of leuco-MB form [56] did not contribute to the UV absorption rising. This means that the portion of MB transferred to leuco-MB is moderately low and that a major quantity of MB is degraded in the alkaline environment by HO_2^- .

Figure 6b depicts a slight effect of adsorption upon rotating the electrode due to increased mass flow of the MB solution towards the electrode. Concurrent adsorption and inherent KOH bleaching decreased the signal by 23.1%. Importantly, this decrease is simultaneously seen for both UV and Vis absorption bands, suggesting an actual MB solution concentration decrease without the evolution of the leuco-MB form.

The intended effect of electrogenerated HO_2^- towards MB degradation is seen by a gross 65.9% calculated from a decrease in MB absorption bands in the 450–750 nm region (42.8% when corrected for inherent degradation and effect of rotation) within an hour when potential is held at -0.8 V, Figure 6c. The results can be interpreted in accordance with the literature whereby MB is positively charged [57], suggesting that it will readily adsorb electrostatically on a negative electrode surface. Maintaining the HO_2^- generation at -0.8 V vs. SCE will have the additional effect of attracting MB towards the surface. Once there, MB will simultaneously adsorb at the electrode and be in close proximity to the generated HO_2^- , a known proton donor, with electrons from the electrode enabling successful MB degradation by demethylation/deamination via OH- and HO_2^- intermediates resulting in colored products (Azure A/B/C and Methylene violet) [50]. A rotating disc electrode (RDE) forces the convection of the MB molecules as well as oxygen from the bulk of the solution towards the electrode surface.

Increased convection results in the formation of significantly more HO_2^- , seen as an increase in measured current, and more MB molecules near the surface. By integrating current with respect to time, the amount of charge spent on HO_2^- generation could be assessed and amounted to (0.46, 0.60 and 0.61 C) recalculated to 2.37, 3.10, and 3.14 μmol of HO_2^- , which was sufficient to account for the decrease in initial MB content (0.18 μmol). The combined effect is the significant decrease in MB concentration indicating successful degradation by in situ electrogenerated nucleophile attack.

Using a test reaction with MB, it was demonstrated that the new carbonized material derived from the saturated adsorbent can be successfully used for the generation of HO_2^- . In addition to bleaching, electro-generated HO_2^- could be used for wider environmental applications, such as a non-selective oxidant in water purification systems.

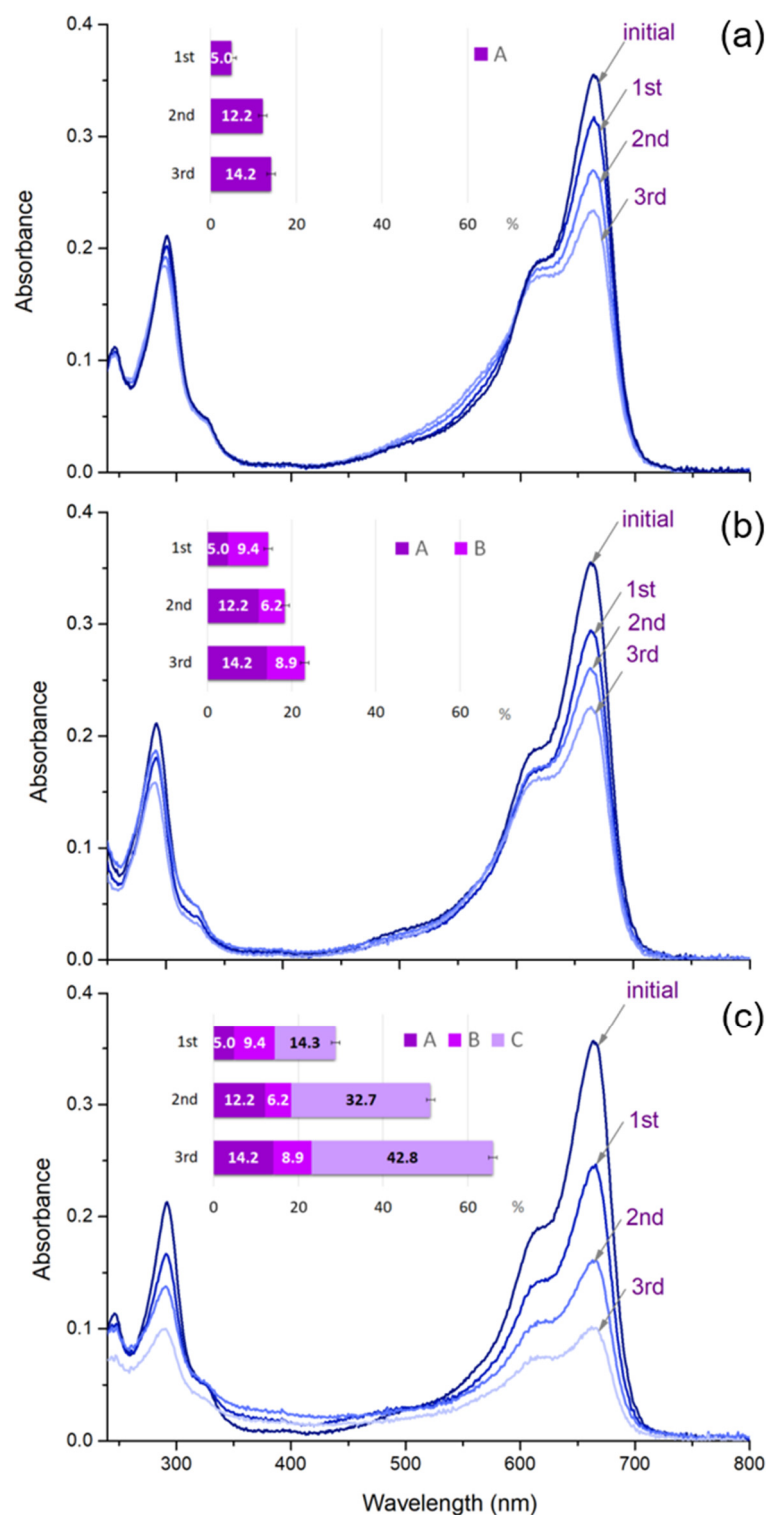


Figure 6. Spectro-electrochemical results on MB degradation in (A) KOH electrolyte (a); (A + B) KOH-filled electrolytic cell with rotating electrode (b) and (A + B + C) KOH-filled electrolytic cell with rotating electrode and potential applied (c).

3. Materials and Methods

3.1. Materials

The natural zeolite, clinoptilolite (CL), used in this study originates from the Zlatokop deposit (Vranje, Serbia). Diatomite samples were examined from two sites, one of domestic origin, the Kolubara basin Serbia (DK), and the other originating from South America,

Peru (DP sample, food-grade diatomaceous earth, freshwater source). The DP sample was neat and used as is, while the DK sample was used after thermal treatment (at 550 °C for 4 h). Bentonite (BE) obtained from Fagron (Greece) and kaolin (KA) from Sigma-Aldrich (St. Louis, MI, USA), were both of the pharmaceutical (Ph. Eur.) grade.

3.2. Characterization of the Natural Silicates

Infrared spectroscopy with Fourier analysis was performed in the range 4000–400 cm^{-1} with 32 scans per spectrum and a 4 cm^{-1} resolution on Nicolet iS20 spectrometer (Thermo Scientific, Waltham, MA, USA) using KBr pellet technique.

X-ray diffraction (XRD) at room temperature was performed on a D8 Advance diffractometer (Bruker, Karlsruhe, Germany) using Cu $K\alpha$ radiation, at a 40 kV voltage and 40 mA current. Diffraction data were collected in the 2–50° 2θ range with a 0.02° step and 0.1 s retention time per step. Data collection was guided by DIFFRAC Plus Commander v.2.6.1 software (Bruker, Germany).

UV–Vis absorption spectra were recorded on an Evolution 220 spectrometer (Thermo Scientific, Waltham, MA, USA) in a quartz cuvette with an optical path of 1 cm or 0.1 cm, in the 200–800 nm range.

The investigated minerals were subjected to thermogravimetry (TG) on thermobalance SDT 2960 (TA Instruments, New Castle, DE, USA). Measurements were performed up to 900 °C with the heating rate 10 °C min^{-1} in a synthetic air atmosphere with a flow rate of 80 mL min^{-1} .

3.3. Methylene Blue Adsorption, Adsorbents Treatment and Characterization

The natural silicates were tested as adsorbents for MB from aqueous solutions. The batch adsorption suspensions comprised 10 mg of solid adsorbent and 5 mL volume of MB (Reag. Ph. Eur., Merck, Kenilworth, NJ, USA) solution. The suspensions were placed in an ultrasonic bath for 2 × 10 min. For lower MB concentrations (20–80 ppm), 1 mL of the suspension was centrifuged for 5 min at 13,400 rpm and UV–Vis spectra were recorded after 1 h equilibration time. In the case of higher concentrations (100–500 ppm), spectra were recorded after 24 h equilibration time.

All samples were tested for adsorption in 100 ppm and 200 ppm MB concentrations. As bentonite was the only material that completely adsorbed 200 ppm MB, this sample was further investigated for retention of higher concentrations—300, 400 and 500 ppm.

Upon adsorption of Methylene Blue, the selected sample was heated in a tubular furnace within argon atmosphere for 2 h at 700 °C, and 10 °C/min rate. The carbonized sample was denoted C-MB@BE.

In addition to FTIR measurements, a DXR Raman spectrometer with a microscope (Thermo Scientific, Waltham, MA, USA), was employed for spectral analysis of carbonized saturated adsorbent. Laser wavelength was 532 nm and power set at 2.0 mW, with 10 × 10 s exposure time, 900 lines/mm grating and 50 μm aperture.

The elemental composition of the carbonized sample was investigated by an energy-dispersive X-ray spectrometer (EDX) coupled with a Phenom ProX scanning electron microscope (Thermo Scientific, Waltham, MA, USA).

3.4. Electrochemical Measurements

Glassy carbon (GC) electrode coated with a thin film of the carbonized sample was used for electrochemical measurements. Liquid ink suspension was arranged by sonicating 5 mg of C-MB@BE in 0.5 mL of ethanol/water/Nafion mixture. Loading of 250 $\mu\text{g cm}^{-2}$ was achieved by drop-casting 5 μL of the suspension on top of the GC disk (5 mm diameter). Oxygen reduction reaction (ORR) activity and MB degradation were evaluated using cyclic voltammetry (CV) in a conventional three-electrode cell with Pt wire as a counter and a saturated calomel electrode (SCE) as a reference electrode, in 0.1 M KOH aqueous solution as supporting electrolyte. An Ivium VO1107 potentiostat/galvanostat was used to impose the desired potential and measure the current response. Before and during the

measurements, slight oxygen flow was kept through the electrolyte to keep the solution saturated with oxygen. The baseline was recorded by purging nitrogen through the cell to eliminate oxygen and concurrently all processes that use oxygen. Measurements were performed at standard pressure and ambient temperature. Koutecký–Levich analysis (K–L) (Equation (1)) was used to define the mechanism of ORR and determine the number of exchanged electrons per oxygen molecule:

$$\frac{1}{i_m} = \frac{1}{i_k} + \frac{1}{B\omega^{1/2}} \quad (1)$$

where i_m is the measured current, i_k is the kinetic current from the electrochemical reaction, B is the Levich constant and ω is the angular rotation rate.

Spectro-electrochemical measurements were performed by dissolving 1 mL of 500 ppm MB aqueous solution in 249 mL 0.1 M KOH. Generation of species was carried out at a constant potential (−0.8 V vs. SCE), at 2400 rpm, with 5 mL aliquots being drawn for UV–Vis measurements every 1200 s, three successive times.

4. Conclusions

Herein, we propose a straightforward selection of the best adsorbent of methylene blue (MB) in aqueous solutions among natural aluminosilicates (bentonite, kaolin, clinoptilolite and diatomites). Nitrogen-rich MB was selected for investigation as a model pollutant in water tables.

Complete MB removal (cca. 95%) was witnessed up to a 500 ppm starting concentration, where 236.6 mg MB was adsorbed per gram of bentonite, while other silicates showed significantly lower capacities. The excellent adsorption performance of bentonite is attributed to its interlayered structure with evenly distributed adsorption sites. The MB interaction with the bentonite sample was confirmed by FTIR analysis along with mineral structure preservation and insight into possible adsorption centers. MB-saturated bentonite was further heated in an inert atmosphere to carbonize the adsorbate. Raman spectral analysis confirmed the amorphous carbon phase on the bentonite sample, and FTIR spectra evidenced the preservation of the aluminosilicate structure. The obtained carbonaceous material comprises N and S as confirmed by the EDX investigation.

The doped carbon material was tested for its activity toward oxygen reduction in an alkaline solution. The Koutecký–Levich analysis confirmed that $2e^-$ are consumed in the selected potential region, therefore, confirming HO_2^- formation. To exploit nucleophile generation, in situ, three complementary experiments were conducted in three 20 min runs. As a baseline, in the absence of rotation, a decrease in MB concentration matches that naturally occurring in an alkaline MB solution in the amount of 14%. In the presence of rotation of the carbonized MB-saturated bentonite electrode, but without the applied potential, MB concentration decreases by 23% due to electrode adsorption in addition to MB alkaline bleaching. Finally, the effect of electrogenerated HO_2^- on MB degradation is seen by a 66% decrease within an hour. For successful MB degradation, the generation of a significant local concentration of HO_2^- is needed in the presence of a reasonable concentration of MB near or at the surface. This local, electro-generated HO_2^- concentration surpasses that found in the solution and successful degradation prefers intimate contact of pollutant molecules and HO_2^- at the electrode surface.

The combined effect of convection and oxygen reduction enables successful degradation of pollutants by in situ electrogenerated nucleophile attack, placing this procedure as a method of choice for spent adsorbent employment.

Supplementary Materials: The following supporting information can be downloaded at: <https://www.mdpi.com/article/10.3390/catal12050519/s1>, Figure S1: XRD pattern of bentonite sample; Figure S2: Calibration curve for MB in (a) an aqueous solution and (b) KOH, based on integral absorption band surface area; Figure S3: Raman and FTIR spectra of carbonized C-MB@BE sample.

Author Contributions: Conceptualization, D.P., M.M.-R. and D.B.-B.; methodology, D.P., D.K., N.G. and L.I.; formal analysis, D.P.; investigation, D.P., S.M. and N.G.; resources, L.I., S.M. and D.K.; data curation, D.P., D.B.-B. and N.G.; writing—original draft preparation, D.P., D.B.-B. and N.G.; writing—review and editing, M.M.-R., D.B.-B. and N.G.; visualization, M.M.-R.; supervision, D.B.-B. and N.G. All authors have read and agreed to the published version of the manuscript.

Funding: This research was funded by the Ministry of Education, Science and Technological Development of the Republic of Serbia, grant numbers 451-03-68/2022-14/200146 and 451-03-68/2022-14/200161.

Data Availability Statement: Data are contained within the article or Supplementary Materials.

Conflicts of Interest: The authors declare no conflict of interest. The funders had no role in the design of the study; in the collection, analyses, or interpretation of data; in the writing of the manuscript, or in the decision to publish the results.

References

1. Ganguly, S.; Das, P.; Das, T.K.; Ghosh, S.; Das, S.; Bose, M.; Mondal, M.; Das, A.K.; Das, N.C. Acoustic Cavitation Assisted De-stratified Clay Tactoid Reinforced in Situ Elastomer-Mimetic Semi-IPN Hydrogel for Catalytic and Bactericidal Application. *Ultrason. Sonochemistry* **2020**, *60*, 104797. [CrossRef]
2. Ganguly, S.; Das, N.C. Water Uptake Kinetics and Control Release of Agrochemical Fertilizers from Nanoclay-Assisted Semi-Interpenetrating Sodium Acrylate-Based Hydrogel. *Polym.-Plast. Technol. Eng.* **2017**, *56*, 744–761. [CrossRef]
3. Krajišnik, D.; Milojević, M.; Malenović, A.A.; Daković, A.; Ibrić, S.; Savić, S.S.; Dondur, V.; Matijašević, S.; Radulović, A.; Daniels, R.; et al. Cationic Surfactants-Modified Natural Zeolites: Improvement of the Excipients Functionality. *Drug Dev. Ind. Pharm.* **2010**, *36*, 1215–1224. [CrossRef] [PubMed]
4. Cerri, G.; Farina, M.; Brundu, A.; Daković, A.; Giunchedi, P.; Gavini, E.; Rassa, G. Natural Zeolites for Pharmaceutical Formulations: Preparation and Evaluation of a Clinoptilolite-Based Material. *Microporous Mesoporous Mater.* **2016**, *223*, 58–67. [CrossRef]
5. Krajišnik, D.; Daković, A.; Malenović, A.; Milojević-Rakić, M.; Dondur, V.; Radulović, Ž.; Milić, J.; Radulović, Z.; Milić, J. Investigation of Adsorption and Release of Diclofenac Sodium by Modified Zeolites Composites. *Appl. Clay Sci.* **2013**, *83–84*, 322–326. [CrossRef]
6. Krajišnik, D.; Daković, A.; Milić, J.; Marković, M. Zeolites as Potential Drug Carriers. In *Modified Clay and Zeolite Nanocomposite Materials*; Elsevier: Amsterdam, The Netherlands, 2019; pp. 27–55.
7. Pagnacco, M.; Maksimović, J.; Mudrinić, T.; Banković, P.; Nedić-Vasiljević, B.; Milutinović-Nikolić, A. Oscillatory Briggs-Rauscher Reaction as “Fingerprint” for Bentonite Identification: The Fine-Tuning of Oscillatory Dynamics with Addition of Clay. *ChemistrySelect* **2020**, *5*, 8137–8141. [CrossRef]
8. Jovic-Jovicic, N.; Bankovic, P.; Mojovic, Z.; Nedic-Vasiljevic, B.; Marinovic, S.; Mudrinic, T.; Milutinovic-Nikolic, A. Ecologically Friendly Chitosan-Montmorillonite Bio-Nanocomposite as Adsorbent for Textile Dyes from Aqueous Solutions. *Sci. Sinter.* **2017**, *49*, 419–429. [CrossRef]
9. Janičijević, J.; Milić, J.; Čalija, B.; Micov, A.; Stepanović-Petrović, R.; Tomić, M.; Daković, A.; Dobričić, V.; Nedić Vasiljević, B.; Krajišnik, D. Potentiation of the Ibuprofen Antihyperalgesic Effect Using Inorganically Functionalized Diatomite. *J. Mater. Chem. B* **2018**, *6*, 5812–5822. [CrossRef] [PubMed]
10. Janičijević, J.; Krajišnik, D.; Čalija, B.; Vasiljević, B.N.; Dobričić, V.; Daković, A.; Antonijević, M.D.; Milić, J. Modified Local Diatomite as Potential Functional Drug Carrier—A Model Study for Diclofenac Sodium. *Int. J. Pharm.* **2015**, *496*, 466–474. [CrossRef]
11. Milojević-Rakić, M.; Popadić, D.; Janošević Ležaić, A.; Jevremović, A.; Nedić Vasiljević, B.; Uskoković-Marković, S.; Bajuk-Bogdanović, D. MFI, BEA and FAU Zeolite Scavenging Role in Neonicotinoids and Radical Species Elimination. *Environ. Sci. Processes Impacts* **2022**, *24*, 265–276. [CrossRef]
12. Barakan, S.; Aghazadeh, V. The Advantages of Clay Mineral Modification Methods for Enhancing Adsorption Efficiency in Wastewater Treatment: A Review. *Environ. Sci. Pollut. Res.* **2021**, *28*, 2572–2599. [CrossRef] [PubMed]
13. Kuang, Y.; Zhang, X.; Zhou, S. Adsorption of Methylene Blue in Water onto Activated Carbon by Surfactant Modification. *Water* **2020**, *12*, 587. [CrossRef]
14. Rosly, N.Z.; Abdullah, A.H.; Ahmad Kamarudin, M.; Ashari, S.E.; Alang Ahmad, S.A. Adsorption of Methylene Blue Dye by Calix [6]Arene-Modified Lead Sulphide (Pbs): Optimisation Using Response Surface Methodology. *Int. J. Environ. Res. Public Health* **2021**, *18*, 397. [CrossRef] [PubMed]
15. Rahmawati, F.; Ridasepri, A.F.; Chairunnisa; Wijayanta, A.T.; Nakabayashi, K.; Miyawaki, J.; Miyazaki, T. Carbon from Bagasse Activated with Water Vapor and Its Adsorption Performance for Methylene Blue. *Appl. Sci.* **2021**, *11*, 678. [CrossRef]
16. Harikishore Kumar Reddy, D.; Vijayaraghavan, K.; Kim, J.A.; Yun, Y.-S. Valorisation of Post-Sorption Materials: Opportunities, Strategies, and Challenges. *Adv. Colloid Interface Sci.* **2017**, *242*, 35–58. [CrossRef]
17. Tian, G.; Wang, W.; Zong, L.; Kang, Y.; Wang, A. From Spent Dye-Loaded Palygorskite to a Multifunctional Palygorskite/Carbon/Ag Nanocomposite. *RSC Adv.* **2016**, *6*, 41696–41706. [CrossRef]

18. Feng, Y.; Dionysiou, D.D.; Wu, Y.; Zhou, H.; Xue, L.; He, S.; Yang, L. Adsorption of Dyestuff from Aqueous Solutions through Oxalic Acid-Modified Swede Rape Straw: Adsorption Process and Disposal Methodology of Depleted Bioadsorbents. *Bioresour. Technol.* **2013**, *138*, 191–197. [[CrossRef](#)]
19. Yan, H.; Zhang, W.; Kan, X.; Dong, L.; Jiang, Z.; Li, H.; Yang, H.; Cheng, R. Sorption of Methylene Blue by Carboxymethyl Cellulose and Reuse Process in a Secondary Sorption. *Colloids Surf. A Physicochem. Eng. Asp.* **2011**, *380*, 143–151. [[CrossRef](#)]
20. Dimitriadis, S.; Nomikou, N.; McHale, A.P. Pt-Based Electro-Catalytic Materials Derived from Biosorption Processes and Their Exploitation in Fuel Cell Technology. *Biotechnol. Lett.* **2007**, *29*, 545–551. [[CrossRef](#)]
21. Zhang, Y.; An, Y.; Wu, L.; Chen, H.; Li, Z.; Dou, H.; Murugadoss, V.; Fan, J.; Zhang, X.; Mai, X.; et al. Metal-Free Energy Storage Systems: Combining Batteries with Capacitors Based on a Methylene Blue Functionalized Graphene Cathode. *J. Mater. Chem. A* **2019**, *7*, 19668–19675. [[CrossRef](#)]
22. Badeenezhad, A.; Azhdarpoor, A.; Bahrami, S.; Yousefinejad, S. Removal of Methylene Blue Dye from Aqueous Solutions by Natural Clinoptilolite and Clinoptilolite Modified by Iron Oxide Nanoparticles. *Mol. Simul.* **2019**, *45*, 564–571. [[CrossRef](#)]
23. Hong, S.; Wen, C.; He, J.; Gan, F.; Ho, Y.-S. Adsorption Thermodynamics of Methylene Blue onto Bentonite. *J. Hazard. Mater.* **2009**, *167*, 630–633. [[CrossRef](#)] [[PubMed](#)]
24. Mouni, L.; Belkhirri, L.; Bollinger, J.-C.; Bouzaza, A.; Assadi, A.; Tirri, A.; Dahmoune, F.; Madani, K.; Remini, H. Removal of Methylene Blue from Aqueous Solutions by Adsorption on Kaolin: Kinetic and Equilibrium Studies. *Appl. Clay Sci.* **2018**, *153*, 38–45. [[CrossRef](#)]
25. Al-Ghouti, M.A.; Khraisheh, M.A.M.; Ahmad, M.N.M.; Allen, S. Adsorption Behaviour of Methylene Blue onto Jordanian Diatomite: A Kinetic Study. *J. Hazard. Mater.* **2009**, *165*, 589–598. [[CrossRef](#)] [[PubMed](#)]
26. Yang, B.; Liu, X.; Ma, Z.; Wang, Q.; Yang, J. Synthesis of Nano-ZnO/Diatomite Composite and Research on Photoelectric Application. *Catalysts* **2021**, *11*, 1232. [[CrossRef](#)]
27. Liu, Y.; Wang, L.; Xue, N.; Wang, P.; Pei, M.; Guo, W. Ultra-Highly Efficient Removal of Methylene Blue Based on Graphene Oxide/TiO₂/Bentonite Sponge. *Materials* **2020**, *13*, 824. [[CrossRef](#)]
28. Kuntubek, A.; Kinayat, N.; Meiramkulova, K.; Pouloupoulos, S.G.; Bear, J.C.; Inglezakis, V.J. Catalytic Oxidation of Methylene Blue by Use of Natural Zeolite-Based Silver and Magnetite Nanocomposites. *Processes* **2020**, *8*, 471. [[CrossRef](#)]
29. Samarghandi, M.R.; Dargahi, A.; Shabanloo, A.; Nasab, H.Z.; Vaziri, Y.; Ansari, A. Electrochemical Degradation of Methylene Blue Dye Using a Graphite Doped PbO₂ Anode: Optimization of Operational Parameters, Degradation Pathway and Improving the Biodegradability of Textile Wastewater. *Arab. J. Chem.* **2020**, *13*, 6847–6864. [[CrossRef](#)]
30. Droguett, T.; Mora-Gómez, J.; García-Gabaldón, M.; Ortega, E.; Mestre, S.; Cifuentes, G.; Pérez-Herranz, V. Electrochemical Degradation of Reactive Black 5 Using Two-Different Reactor Configuration. *Sci. Rep.* **2020**, *10*, 4482. [[CrossRef](#)]
31. Łuba, M.; Mikołajczyk, T.; Pierożyński, B.; Smoczyński, L.; Wojtacha, P.; Kuczyński, M. Electrochemical Degradation of Industrial Dyes in Wastewater through the Dissolution of Aluminum Sacrificial Anode of Cu/Al Macro-Corrosion Galvanic Cell. *Molecules* **2020**, *25*, 4108. [[CrossRef](#)]
32. Irfan Khan, M.; Khan, H.U.; Azizli, K.; Sufian, S.; Man, Z.; Siyal, A.A.; Muhammad, N.; Faiz ur Rehman, M. The Pyrolysis Kinetics of the Conversion of Malaysian Kaolin to Metakaolin. *Appl. Clay Sci.* **2017**, *146*, 152–161. [[CrossRef](#)]
33. Bourliva, A.; Michailidis, K.; Sikalidis, C.; Filippidis, A. Spectroscopic and Thermal Study of Bentonites from Milos Island, Greece. *Bull. Geol. Soc. Greece* **2013**, *47*, 2020. [[CrossRef](#)]
34. Krajišnik, D.; Daković, A.; Milojević, M.; Malenović, A.; Kragović, M.; Bajuk-Bogdanović, D.; Dondur, V.; Milić, J. Properties of Diclofenac Sodium Sorption onto Natural Zeolite Modified with Cetylpyridinium Chloride. *Colloids Surf B Biointerfaces* **2011**, *83*, 165–172. [[CrossRef](#)] [[PubMed](#)]
35. Farmer, V.C. Transverse and Longitudinal Crystal Modes Associated with OH Stretching Vibrations in Single Crystals of Kaolinite and Dickite. *Spectrochim. Acta Part A Mol. Biomol. Spectrosc.* **2000**, *56*, 927–930. [[CrossRef](#)]
36. Russell, J.D.; Fraser, A.R. Infrared Methods. In *Clay Mineralogy: Spectroscopic and Chemical Determinative Methods*; Springer: Dordrecht, The Netherlands, 1994; pp. 11–67.
37. El Ouardi, Y.; Branger, C.; Toufik, H.; Laatikainen, K.; Ouammou, A.; Lenoble, V. An Insight of Enhanced Natural Material (Calcined Diatomite) Efficiency in Nickel and Silver Retention: Application to Natural Effluents. *Environ. Technol. Innov.* **2020**, *18*, 100768. [[CrossRef](#)]
38. Zaitan, H.; Bianchi, D.; Achak, O.; Chafik, T. A Comparative Study of the Adsorption and Desorption of O-Xylene onto Bentonite Clay and Alumina. *J. Hazard. Mater.* **2008**, *153*, 852–859. [[CrossRef](#)]
39. Jović-Jovičić, N.; Milutinović-Nikolić, A.; Banković, P.; Dojčinović, B.; Nedić, B.; Gržetić, I.; Jovanović, D. Synthesis, Characterization and Adsorptive Properties of Organobentonites. *Acta Phys. Pol. A* **2010**, *117*, 849–854. [[CrossRef](#)]
40. Zhirong, L.; Azhar Uddin, M.; Zhanxue, S. FT-IR and XRD Analysis of Natural Na-Bentonite and Cu(II)-Loaded Na-Bentonite. *Spectrochim. Acta Part A Mol. Biomol. Spectrosc.* **2011**, *79*, 1013–1016. [[CrossRef](#)]
41. Madejová, J.; Gates, W.P.; Petit, S. IR Spectra of Clay Minerals. In *Developments in Clay Science*; Elsevier: Amsterdam, The Netherlands, 2017; pp. 107–149.
42. Faghihian, H.; Kabiri-Tadi, M. Removal of Zirconium from Aqueous Solution by Modified Clinoptilolite. *J. Hazard. Mater.* **2010**, *178*, 66–73. [[CrossRef](#)]
43. Fernández-Pérez, A.; Valdés-Solís, T.; Marbán, G. Visible Light Spectroscopic Analysis of Methylene Blue in Water; the Resonance Virtual Equilibrium Hypothesis. *Dye. Pigment.* **2019**, *161*, 448–456. [[CrossRef](#)]

44. Kahr, G.; Madsen, F.T. Determination of the Cation Exchange Capacity and the Surface Area of Bentonite, Illite and Kaolinite by Methylene Blue Adsorption. *Appl. Clay Sci.* **1995**, *9*, 327–336. [[CrossRef](#)]
45. Yang, R.T. *Adsorption: Fundamentals and Applications*; Wiley-Interscience: Hoboken, NJ, USA, 2003; ISBN 0-471-29741-0.
46. Rupar, J.; Bajuk-Bogdanović, D.; Milojević-Rakić, M.; Krstić, J.; Upadhyay, K.; Gavrilov, N.; Janošević Ležaić, A. Tailored Porosity Development in Carbons via Zn²⁺ Monodispersion: Fitting Supercapacitors. *Microporous Mesoporous Mater.* **2022**, *335*, 111790. [[CrossRef](#)]
47. Gavrilov, N.; Pašti, I.A.; Mitrić, M.; Travas-Sejdić, J.; Ćirić-Marjanović, G.; Mentus, S.V. Electrocatalysis of Oxygen Reduction Reaction on Polyaniline-Derived Nitrogen-Doped Carbon Nanoparticle Surfaces in Alkaline Media. *J. Power Sources* **2012**, *220*, 306–316. [[CrossRef](#)]
48. Chen, Z.; Zheng, R.; Wei, W.; Wei, W.; Zou, W.; Li, J.; Ni, B.-J.; Chen, H. Recycling Spent Water Treatment Adsorbents for Efficient Electrocatalytic Water Oxidation Reaction. *Resour. Conserv. Recycl.* **2022**, *178*, 106037. [[CrossRef](#)]
49. Pérez-Díaz, P.J.; Medina-Ramírez, A.; Esquivel, I.R.G.; Ruiz, G.G.; Ruiz-Camacho, B. Effect of X Zeolite-Carbon Composite Ratio as Support of Pt Nanoparticles for MOR and ORR. *Ionics* **2021**, *27*, 1813–1828. [[CrossRef](#)]
50. Katafias, A.; Lipińska, M.; Strutyński, K. Alkaline Hydrogen Peroxide as a Degradation Agent of Methylene Blue—Kinetic and Mechanistic Studies. *React. Kinet. Mech. Catal.* **2010**, *101*, 251–266. [[CrossRef](#)]
51. Zhan, R.; Song, S.; Liu, Y.; Dong, S. Mechanisms of Methylene Blue Electrode Processes Studied by in Situ Electron Paramagnetic Resonance and Ultraviolet-Visible Spectroelectrochemistry. *J. Chem. Soc. Faraday Trans.* **1990**, *86*, 3125–3127. [[CrossRef](#)]
52. Adamčíková, L.; Pavlíková, K.; Ševčík, P. The Decay of Methylene Blue in Alkaline Solution. *React. Kinet. Catal. Lett.* **2000**, *69*, 91–94. [[CrossRef](#)]
53. Salamifar, S.E.; Mehrgardi, M.A.; Kazemi, S.H.; Mousavi, M.F. Cyclic Voltammetry and Scanning Electrochemical Microscopy Studies of Methylene Blue Immobilized on the Self-Assembled Monolayer of n-Dodecanethiol. *Electrochim. Acta* **2010**, *56*, 896–904. [[CrossRef](#)]
54. Kelley, S.O.; Barton, J.K.; Jackson, N.M.; Hill, M.G. Electrochemistry of Methylene Blue Bound to a DNA-Modified Electrode. *Bioconjugate Chem.* **1997**, *8*, 31–37. [[CrossRef](#)]
55. Begum, R.; Najeeb, J.; Sattar, A.; Naseem, K.; Irfan, A.; Al-Sehemi, A.G.; Farooqi, Z.H. Chemical Reduction of Methylene Blue in the Presence of Nanocatalysts: A Critical Review. *Rev. Chem. Eng.* **2020**, *36*, 749–770. [[CrossRef](#)]
56. Pegu, R.; Majumdar, K.J.; Talukdar, D.J.; Pratihar, S. Oxalate Capped Iron Nanomaterial: From Methylene Blue Degradation to Bis(Indolyl)Methane Synthesis. *RSC Adv.* **2014**, *4*, 33446–33456. [[CrossRef](#)]
57. Wei, X.; Wang, Y.; Feng, Y.; Xie, X.; Li, X.; Yang, S. Different Adsorption-Degradation Behavior of Methylene Blue and Congo Red in Nanoceria/H₂O₂ System under Alkaline Conditions. *Sci. Rep.* **2019**, *9*, 4964. [[CrossRef](#)] [[PubMed](#)]